Quantum-walk-based search and centrality

Scott D. Berry* and Jingbo B. Wang†
School of Physics, The University of Western Australia, Perth, WA 6009, Australia
(Received 1 September 2010; published 26 October 2010)

We study the discrete-time quantum-walk-based search for a marked vertex on a graph. By considering various structures in which not all vertices are equivalent, we investigate the relationship between the successful search probability and the position of the marked vertex, in particular, its centrality. We find that the maximum value of the search probability does not necessarily increase as the marked vertex becomes more central, and we investigate an interesting relationship between the frequency of the successful search probability and the centrality of the marked vertex.

DOI: 10.1103/PhysRevA.82.042333 PACS number(s): 03.67.Ac

I. INTRODUCTION

Quantum walks are the quantum analog of classical random walks. Rather than stepping with a certain probability between adjacent vertices of a graph, a quantum walker is characterized by a set of probability amplitudes associated with vertices of the graph [1]. The strikingly different behavior of quantum walks from their classical counterparts has already been harnessed in the formulation of quantum-walk-based algorithms that can outperform corresponding classical algorithms [2–4]. While the continued interest in quantum walks is largely due to these algorithmic applications in the context of quantum computation, the quantum walk also forms a powerful and flexible model of the evolution of a coherent (or partially decoherent) quantum system [5–9]. Since analytical techniques are currently being developed to analyze quantum walks, their application to diverse problems in physics will likely become increasingly common. Given also the usefulness of classical random walks in studying transport on complex structures, it is interesting from a physical standpoint to continue to characterize quantum walks on graphs.

Searching is one of the major problems in computer science and a large amount of research in the field of theoretical quantum computation has been in the development of general algorithms for fast searching of databases. Quantum search algorithms were first introduced by Grover to search an unsorted database [10,11] and later extended to quantum-walk-based search algorithms for specific database topologies in both the discrete-time [12–14] and the continuous-time [15] cases. These studies focused on highly symmetric structures such as hypercubic lattices, complete graphs, and bipartite graphs and found that the topology of the database was crucial in determining the efficiency of the search. An important difference between the discrete- and the continuous-time formulations of quantum walks is the extra "coin" degrees of freedom in the discrete-time case. Ambainis *et al.* [13] demonstrated that discrete-time search can achieve full quadratic speedup relative to classical search for hypercubic lattices in three or more dimensions and it outperforms continuous-time search for lattices in two spatial dimensions. As shown by Childs and Goldstone [15], continuous-time search on the hypercube only achieves the full quadratic speedup for d-dimensional lattices where $d > 4$.

A recent paper by Agliari *et al.* [16] considers continuous-time quantum-walk-based search on fractals and thus represents the first effort to characterize the search procedure on structures that are not vertex-transitive. An interesting phenomenon which arises when studying structures where not all vertices are equivalent is that the successful search probability depends on the location of the marked vertex. In their study of quantum search on Cayley trees, T fractals, and dual Sierpiński gaskets, Agliari *et al.* assumed that a peripheral vertex would be more difficult to find than a more central vertex, that is, the maximum success probability for a central vertex would be greater than for a peripheral vertex. In this work, we analyze this idea in more detail by studying how the maximum success probability varies with the centrality of the marked vertex. We find that in some simple cases, the maximum success probability does indeed increase with increasing centrality. However, we show that, in general, such a relationship does not hold.

The efficiency of quantum-walk-based search relative to classical search is determined not only by the maximum success probability, but also by the time taken to reach the maximum. We therefore analyze the lowest frequency of the success probability as an indicator of the time complexity of the search. Our results suggest that this frequency is correlated with the centrality for a larger class of graphs than the maximum success probability and we discuss exceptions in terms of local structure of these graphs.

In this article, we study discrete-time quantum-walk-based search on non-vertex-transitive structures and show that the frequencies present in the success probability are determined by the global structure of the graph as well as the centrality and local structure surrounding the marked vertex. Our derivation in the Appendix contains an analytical solution for discrete-time quantum-walk-based search on a finite line with two reflecting boundaries, which provides the characteristic frequencies of the success probability.

The article is organized as follows. Section II provides an introduction to quantum walks and quantum-walk-based search. Section III describes the measure of centrality used. In Sec. IV we describe the structures considered and in Secs. V, VI, and VII we present our analytical and numerical results. Finally, Sec. VIII contains discussion and conclusions. In the Appendix we provide details of our analytical calculations.

*berrys01@student.uwa.edu.au
†wang@physics.uwa.edu.au

II. QUANTUM-WALK-BASED SEARCH ON GRAPHS

Let $G(V,E)$ be an undirected graph with vertex set $V=\{v_1,v_2,v_3,\ldots\}$ and edge set $E=\{(v_i,v_j),(v_k,v_l),\ldots\}$ consisting of unordered pairs of connected vertices. If there are d edges incident on a vertex v_i, we say that v_i has degree d. As described in [17] and [18], $\mathcal{H}_\mathcal{P}$ is defined as the position Hilbert space, which is spanned by an orthonormal basis of vertex states $\{|v_i\rangle : v_i \in V\}$. For a graph of maximum degree d, $\mathcal{H}_\mathcal{C}$ is defined as the d-dimensional coin Hilbert space spanned by the orthonormal basis of coin states $\{|c_i\rangle : i=1,\ldots,d\}$, representing the outgoing edges at a vertex v_i. The discrete-time quantum walk considered here takes place on the subnodes of the graph, which are represented by product states of the form $|v\rangle\otimes|c\rangle=|v,c\rangle\in\mathcal{H}_\mathcal{P}\otimes\mathcal{H}_\mathcal{C}$. Note that if G is not d-regular, then there are vertices of degree $d_i<d$. In this case the states $\{|v_i,c\rangle : c>d_i\}$ do not physically represent subnodes of the graph G and are not occupied at any stage of a quantum walk on G.

Let one step of the discrete-time quantum walk on the graph be the application of the unitary time-evolution operator $U=S(\mathbb{1}\otimes C)$, where S is the shift operator and C is the coin operator. S acts on the extended position space $\mathcal{H}_\mathcal{P}\otimes\mathcal{H}_\mathcal{C}$ as

$$S|v_i,c_j\rangle=|v_j,c_i\rangle, \tag{1}$$

where $|v_i,c_j\rangle$ is the subnode state corresponding to the edge (v_i,v_j) at vertex v_i. The coin operator C at a vertex v_i of degree d_i can be represented by a $d_i\times d_i$ matrix, which mixes the probability amplitudes of the subnode states of v_i. We mainly consider symmetric coin matrices, so that the ordering of the subnodes at a particular vertex is unimportant. In the Appendix, when we reduce the quantum walk on a Cayley tree to a one-dimensional walk, we need a biased coin. The labeling will then become important and will be made explicit.

We follow the procedure introduced by Shenvi *et al.* [12] for the discrete-time quantum-walk-based search for a marked item. The quantum walker initially has equal probability to be found at each vertex; that is, the state $|\Psi_0\rangle$ is an equal superposition of all vertex states $|v_i\rangle\in\mathcal{H}_\mathcal{P}$. The probability amplitude at each vertex is then divided equally between all subnodes. It should be noted that for a graph which is not degree-regular, this is *not* the same as an equal superposition of all subnode states. Formally, the initial state is given by

$$|\Psi_0\rangle=\frac{1}{\sqrt{N}}\sum_{i=1}^{N}\sum_{j=1}^{d_i}\frac{1}{\sqrt{d_i}}|v_i,c_j\rangle. \tag{2}$$

Now consider a subset $M\subset V$ of *marked vertices*. The marking is intended to represent a "quantum oracle" and is implemented as a perturbation to the coin operator at the marked vertices. A precise description of an oracle in this context is given in [12]. The quantum search procedure proceeds via the repeated application of the perturbed time-evolution operator, $U'=S(\mathbb{1}\otimes C')$, where the coin operator at vertex v_i is given by

$$(C'_i)_{mn}=\begin{cases}-\delta_{mn}+2/d_i, & v_i\notin M,\\ -\delta_{mn}, & v_i\in M,\end{cases}\qquad \text{for}\quad m,n=1,\ldots,d_i. \tag{3}$$

The coin operator in Eq. (3) for $v_i\notin M$ is referred to as the Grover coin. For all examples in this paper, the set M will contain only one vertex. The success probability $P_s(t)$ is defined as the probability of finding the quantum walker at the marked vertex v_m at time t. This is given by

$$P_s(t):=|\langle v_m|\Psi(t)\rangle|^2=|\langle v_m|(U')^t|\Psi_0\rangle|^2,\quad \text{where}\quad v_m\in M. \tag{4}$$

The time-averaged success probability is denoted $\langle P_s\rangle$. As shown in Eq. (4), $P_s(t)$ is determined by unitary time evolution from the initial state. Reversibility of unitary processes implies that $P_s(t)$ does not converge for large t but instead oscillates, which allows us to define the search frequency ω_s as the lowest frequency present in the success probability. In graphs for which quantum walks are not exactly periodic, this is computed from the power spectrum of $P_s(t)$ by selecting the lowest frequency above noise. Assuming that the sample time is sufficient that the Fourier transform has converged, we define the threshold as 10% of the highest peak present in the power spectrum. For the simple graphs studied here the power spectra computed contain only a few frequencies and this functional definition is adequate. We expect, however, that for graphs with less symmetry the threshold may need to be modified.

Using ω_s it is possible to determine the "period" of $P_s(t)$, that is, the approximate integer time difference between minima in $P_s(t)$. To be of any use in the search context the search probability must reach a high value during the first period. We therefore quantify the success of the search as $P_{\max}:=\max\{P_s(t) : 1\leqslant t\leqslant 2\pi/\omega_s, t\in\mathbb{Z}\}$.

The quantum search procedure resembles the wavelike propagation of a (phase-inverted) perturbation over a graph. The perturbation originates from the marked vertex at each time step and results in time-dependent amplitude amplification at the marked vertex, measured by $P_s(t)$. The maxima in $P_s(t)$ occur when the probability amplitudes constructively interfere at the marked vertex, which is highly dependent on the structure of the graph. The amplitude and time dependence of $P_s(t)$ are therefore determined by both the local and the global structure of the graph. In turn, these quantities may be used to provide information about this underlying structure. Indeed, using a similar procedure, Douglas and Wang [19] gave evidence that the information contained in these amplitudes was sufficient to distinguish pairs of nonisomorphic graphs for all cases tested. It is reasonable therefore to expect that the centrality of a vertex should affect both $P_{\max}$ and ω_s.

III. CENTRALITY

We now define the measure of centrality considered in this paper. The random walk centrality (RWC), introduced by Noh and Reiger [20], is a measure of centrality designed to represent the relative speed with which a given vertex can receive and send information over a network. $P_{ij}(t)$ is defined as the probability of a classical random walker starting at vertex v_i to be at vertex v_j after a time t. The RWC of a vertex v_j is then defined as

$$\mathrm{RWC}_j:=\frac{P_j^\infty}{\tau_j}, \tag{5}$$

where $\tau_j = \sum_{t=0}^{\infty}\{P_{jj}(t) - P_j^{\infty}\}$ and $P_j^{\infty} := \lim_{t\to\infty} P_{ij}(t)$, which is the same for all i. $P_{ij}(t)$ is calculated using the master equation,

$$P_{ij}(t+1) = \sum_k \frac{A_{kj}}{d_k} P_{ik}(t). \tag{6}$$

Here A is the adjacency matrix of the graph and d_k is the degree of vertex v_k. This definition was proposed in the context of complex networks and there is an implicit assumption that the expression for τ_j converges, that is, $\lim_{t\to\infty} P_{ij}(t)$ exists. The master equation [Eq. (6)] describes a random walker that changes its location at each time step. Therefore, for graphs which contain closed walks of only even length, only sites at even distances from the start site are occupied after even times. In this case the probability distribution does not converge, which prevents the calculation of τ_j [Eq. (5)]. This difficulty is easily overcome by redefining the master equation in terms of the *lazy* random walk, such that the lazy random walker only moves at each time step with a probability of $1/2$. This leads to the following master equation:

$$P_{ij}(t+1) = \frac{1}{2}\sum_k \left(\delta_{kj} + \frac{A_{kj}}{d_k}\right) P_{ik}(t). \tag{7}$$

In this case, $\lim_{t\to\infty} P_{ij}(t) = d_j/N$ for all connected graphs regardless of the initial state [21]. On the Sierpiński gasket, where both the lazy RWC and the normal RWC are defined, we find that they show the same qualitative behavior. For the remainder of the paper, RWC refers to the lazy RWC. RWC is an example of a closeness centrality measure, in that larger values of RWC are associated with closeness to the center of a network [22].

IV. TOPOLOGY AND CONNECTIVITY OF GRAPHS CONSIDERED

We now describe the structures considered in this study. The nth generation d-Cayley tree (as shown in Fig. 1) is a tree of n levels in which all vertices in the interior have degree $d_i = d$. The outermost layer of the tree is called the *surface*. All vertices on the surface are called *leaves* and have $d_i = 1$. The total number of vertices in a Cayley tree is $N = [d(d-1)^n - 2]/(d-2)$. The structure is defined more

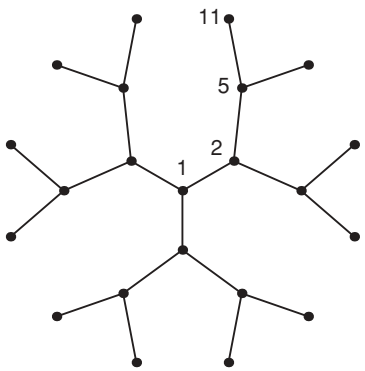

FIG. 1. The third generation 3-Cayley tree. Vertices are ranked and labeled according to their random walk centrality. Nonlabeled vertices are structurally equivalent to one of the labeled vertices.

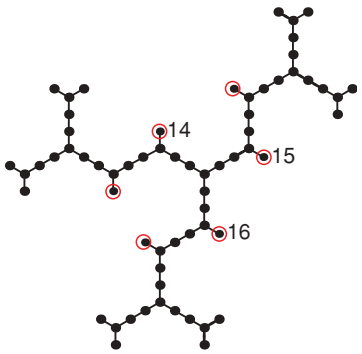

FIG. 2. (Color online) Third-generation regular hyperbranched fractal of functionality $f = 3$ ($\mathrm{RHF}_{3,3}$). Cul-de-sac vertices are highlighted.

rigorously in the Appendix. Quantum walks on Cayley trees, or the closely related "glued-trees" graph of Childs *et al.* have been extensively studied in continuous time [16,23–26], and discrete time [27–29], but not yet for discrete-time quantum search using marking operators.

A first-generation regular hyperbranched fractal (RHF) (as shown in Fig. 2) of functionality f is a star graph consisting of a central vertex connected through f edges to f surface vertices. To construct a second-generation RHF, f copies of the first-generation RHF are connected to the core first-generation RHF through a single leaf-leaf edge. This procedure is repeated n times for an nth-generation RHF. The number of vertices in an RHF therefore grows exponentially with the generation and is given by the formula $N = (f+1)^n$. The maximum degree of a vertex in an RHF is f. Star graphs ($\mathrm{RHF}_{1,f}$) and other $\mathrm{RHF}_{n,f}$ have been studied previously for continuous-time quantum walks in [30] and [31] but not for discrete-time quantum walks.

While the first-generation Cayley trees and $\mathrm{RHF}_{1,f}$ are identical, the structures are distinct for $n > 1$. An important difference in the context of this study is that for $n > 2$, RHFs contain so-called cul-de-sac vertices, which are leaves that are connected to main paths. Note that we do not consider the leaves of the Cayley tree to be cul-de-sac vertices since their neighbors do not lie on main paths.

We also study structures that contain more than one simple path between all pairs of vertices. Specifically, we consider the *joined* Cayley tree, the Husimi cactus, and the Sierpiński gasket. The joined Cayley tree is obtained from the Cayley tree by adding edges between surface vertices (as shown in Fig. 3). For trees with $d = 3$ this results in a 3-regular graph. The Husimi cactus (Fig. 4) is a dual structure to the Cayley tree, constructed by placing a vertex at each edge of the corresponding Cayley tree and connecting vertices that represent adjacent edges in the Cayley tree [32]. The second-generation Sierpiński gasket is shown in Fig. 5 and the structural details are explained in detail in [33]. The number of vertices of an nth-generation Sierpiński gasket is $N = \frac{3}{2}(3^n + 1)$.

V. QUANTUM SEARCH ON CAYLEY TREES

First, we provide an example of the success probabilities obtained for two inequivalent vertices in a Cayley tree. We then

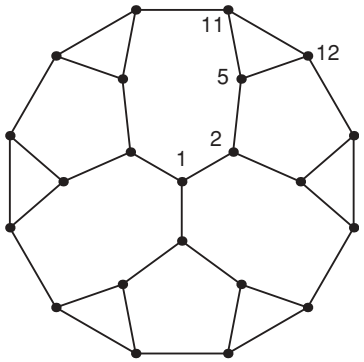

FIG. 3. Third-generation *joined* 3-Cayley tree obtained from the equivalent Cayley tree by connecting surface vertices. Vertices are labeled as for the equivalent Cayley tree. Nonlabeled vertices are structurally equivalent to one of the labeled vertices.

present analytical results for the success probability $P_s(t)$ for the d-Cayley tree when the central vertex is marked. Numerical results are then presented for $P_{\max}$ and ω_s on various Cayley trees when a noncentral vertex is marked. These results are compared with the centrality of the marked vertex. For all simulations in Secs. V, VI, and VII, the initial state is given by Eq. (2).

A. Quantum-walk-based search characteristics

We begin with an example of the success probability obtained on the third-generation 3-Cayley tree (structure shown in Fig. 1). Figure 6(a) shows the success probability $P_s(t)$ as a function of time when the central vertex is marked. Figure 6(b) shows $P_s(t)$ for a peripheral marked vertex in the same graph. Comparing these plots, it can be seen that $P_s(t)$ is quasiperiodic in both cases, with a smaller "period" when the central vertex is marked in comparison with a peripheral marked vertex. $P_s(t)$ also has a greater maximum and average amplitude for the central marked vertex. In the following, we examine how the lowest frequency ω_s and the maximum amplitude $P_{\max}$ vary on Cayley trees.

B. Central marked vertex

In the Appendix we show that a quantum walk on an nth generation d-Cayley tree can be mapped to a one-dimensional

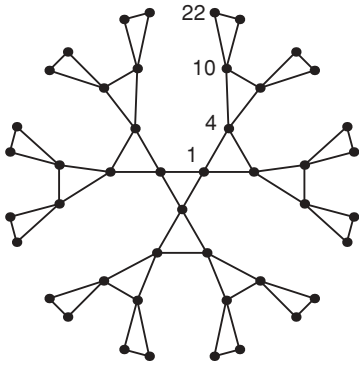

FIG. 4. The $N = 45$ Husimi cactus obtained as a dual structure to the fourth-generation 3-Cayley tree. Vertices are ranked and labeled according to their random walk centrality. Nonlabeled vertices are structurally equivalent to one of the labeled vertices.

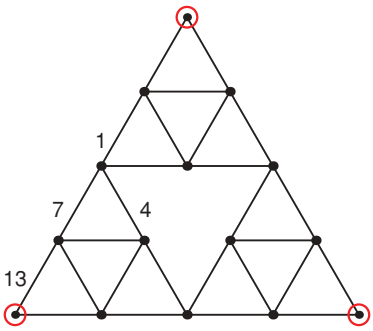

FIG. 5. (Color online) Second-generation Sierpiński gasket. Vertices are ranked and labeled according to their random walk centrality (RWC). Nonlabeled vertices are structurally equivalent to one of the labeled vertices. Highlighted vertices are peripheral (least central as measured by the RWC).

quantum walk. We then study a finite one-dimensional walk with two reflecting boundaries to derive the following expression for ω_s:

$$\omega_s = \omega_s(n,d) := \arctan\left(\frac{2\sqrt{d^{n-1}-1}}{d^{n-1}-2}\right) \quad \text{for} \quad n = 2,3 \quad \text{and} \quad 3 \leqslant d < \infty. \tag{8}$$

This expression is plotted in Fig. 7(a) together with our numerical results obtained by direct simulation of discrete-time quantum search. The numerical and analytical results are in perfect agreement. Finding analytical solutions for ω_s becomes more difficult for $n \geqslant 4$, as large matrices must be diagonalized. For the second-generation Cayley tree ($n = 2$), we are able to derive (see Appendix) the following expression for $P_s(t)$, valid for $3 \leqslant d < \infty$:

$$\begin{aligned} |\langle \mathbb{1}|\Psi(t)\rangle|^2 = \frac{1}{4(1+d^2)}\{&1 + d^2 + (d-1)^2\cos(\pi t) \\ &- (d^2-1)\cos(\omega_s t) + 2\sqrt{d(d-1)}\sin(\omega_s t) \\ &- (d^2-2d-1)\cos[(\pi-\omega_s)t] \\ &- 2\sqrt{d(d-1)}\sin[(\pi-\omega_s)t]\}. \end{aligned} \tag{9}$$

As can be seen from Eq. (9), $P_s(t)$ contains only three frequencies: π, ω_s, and $\pi - \omega_s$. It is interesting to note that $\omega_s(2,4) = \pi/3$, which means that the only frequencies present in $P_s(t)$ are $\{\pi/3, 2\pi/3, \pi\}$. Thus $P_s(t)$ is exactly periodic with period 6.

The search frequencies $\omega_s(2,d)$ and $\omega_s(3,d)$ are plotted in Fig. 7(a). Although for fixed n the distance between the central node and the surface is fixed, it can be seen from Fig. 7(a) that $\omega_s(n,d)$ decreases monotonically with increasing branching rate. According to Eq. (8), for large d, ω_s tends toward 0. This is consistent with the results of Carneiro *et al.* [29], who generalized a discrete-time formulation of Childs' *glued-trees* algorithm [23] to include arbitrary branching rate d and found that as $d \to \infty$, a quantum walker initially localized at the central node of the tree oscillates between the central node and the first level of the tree. While it is not strictly valid to compare absolute values of RWC among different graphs, we find numerically that the RWC of the central vertex of a Cayley tree is also a monotonically decreasing function of d for fixed

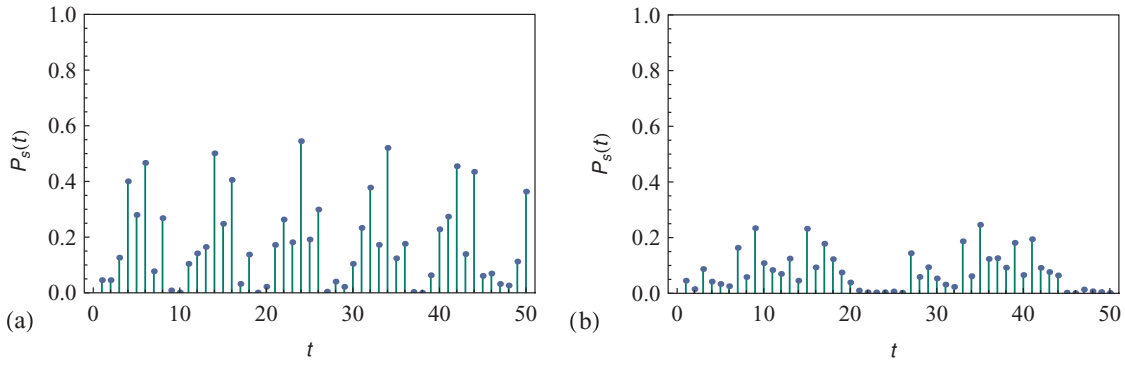

FIG. 6. (Color online) (a) Numerical results for the success probability $P_s(t)$ for the third-generation 3-Cayley tree (structure shown in Fig. 1) when the central vertex is marked (vertex 1). (b) $P_s(t)$ for a peripheral marked vertex (vertex 11) on the same graph.

n, as shown in Fig. 7(b). In this sense, ω_s shows the same behavior as RWC for the central marked vertex of a Cayley tree.

For $n \geqslant 4$ we have numerical results only for ω_s, which are shown in Fig. 8(a). The search frequency ω_s on a Cayley tree with a central marked vertex decreases as the number of generations in the tree increases. Thinking of the search procedure as generating a phase-inverted perturbation at the center of the graph at each time step, these perturbations must constructively interfere at the center of the graph to produce a maximum in $P_s(t)$. To constructively interfere, these perturbations must be reflected at the surface, and thus the time between maxima in $P_s(t)$ depends on the distance between the central vertex and the surface of the graph, which increases with the number of generations, n. As shown in Fig. 8(b), the RWC of the central vertex decreases monotonically with n for fixed d and thus displays the same behavior as ω_s for the Cayley tree.

We now study how $P_{\max}$ varies with d for a central marked vertex in the second-generation Cayley tree. By evaluating Eq. (9) at integers $t \approx \pi/\omega_s(2,d)$, we can find $P_{\max}$ for arbitrary d. The results are shown in Fig. 9 for $3 \leqslant d \leqslant 40$. Numerical results agree with our analytical results for $3 \leqslant d \leqslant 10$. Figure 9 shows that $P_{\max}$ has a much more complex dependence on d than was seen for ω_s. This complex dependence on d arises because the frequencies π, $\omega_s(d)$, and $\pi - \omega_s(d)$ present in $P_s(t)$ do not necessarily constructively interfere within the first period for all d. While the RWC and ω_s both decrease with increasing branching rate, we see that $P_{\max}$ generally becomes larger as d increases. This can be understood as arising from the greater localization of the quantum walk close the central vertex as the branching rate increases.

C. Noncentral marked vertices

The analysis in the Appendix is dependent on being able to map the quantum walk on a Cayley tree to a walk on a line. When a noncentral vertex is marked, the same mapping cannot be used and we do not have analytical results.

Instead we present numerical results for $P_{\max}$ and ω_s on Cayley trees where the marked vertex is not necessarily central. $P_s(t)$ was computed via direct application of U to the probability amplitudes of the subnode states $|v_i,c_j\rangle$ on which the quantum walk takes place. Numerical methods were then used to compute the discrete Fourier transform and ω_s was obtained as defined in Sec II. For a given graph, this was repeated for all possible positions of the marked vertex. Figure 10 shows the dependence of $P_{\max}$ and ω_s on the centrality of the marked vertex for the third-generation Cayley tree with $d = 3$ (structure shown in Fig. 1). As shown in Fig. 10, a more central vertex in a Cayley tree gives rise

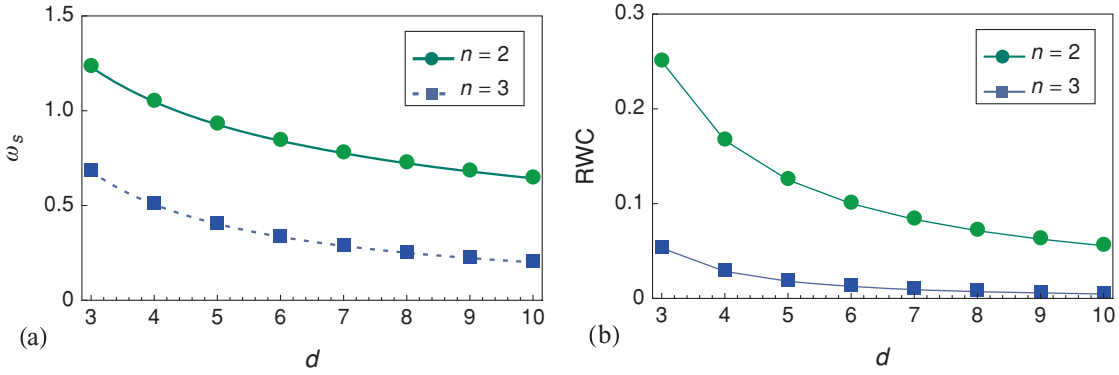

FIG. 7. (Color online) (a) Analytically obtained curves for the search frequency $\omega_s(n,d)$ on a Cayley tree of $n = 2$ and 3 levels with a central marked vertex. Also plotted are numerical data obtained by direct simulation of discrete-time quantum search. (b) random-walk centrality for the central vertex in the same Cayley trees.

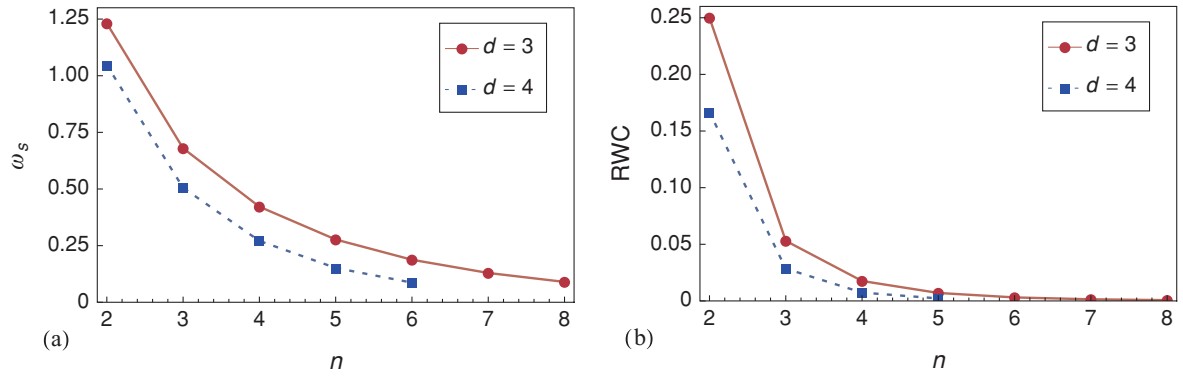

FIG. 8. (Color online) (a) Numerical results for the search frequency ω_s on a Cayley tree with a central marked vertex. ω_s is plotted as a function of the number of generations n, for $d = 3$ (solid line with circles) and $d = 4$ (dashed line with squares). (b) random-walk centrality for the central vertex in the same Cayley trees.

to a success probability $P_s(t)$ which has a larger minimum frequency ω_s and attains a greater maximum amplitude $P_{\max}$. The results for all other Cayley trees studied were analogous.

On Cayley trees, the RWC becomes smaller for vertices which are farther from the central vertex because a random walker starting from a less central vertex takes, on average, longer to visit all vertices. We studied numerically the following Cayley trees: $\{d = 3, n \in [2,8]\}$, $\{d \in [4,5], n \in [2,5]\}$, and $\{d \in [6,10], n \in [2,3]\}$. For all Cayley trees tested we found that $P_{\max}$, $\langle P_s \rangle$, and ω_s decrease monotonically with RWC.

These results are consistent with those observed by Mülken *et al.* [24], who modeled exciton transport on Cayley trees by continuous-time quantum walk and found that excitations which were initially centrally located propagated throughout the structure much more rapidly than excitations which were initially peripheral.

VI. QUANTUM SEARCH ON REGULAR HYPERBRANCHED FRACTALS

We now study RHFs to investigate how greater structural complexity affects both $P_{\max}$ and ω_s. First, we consider the simple case of $n = 2, f = 3$ ($\mathrm{RHF}_{2,3}$). As shown in Fig. 11, the only difference between this fractal and the second-generation 3-Cayley tree is extra vertices of degree 2 on each branch, between the central vertex and level 1. In this case, as for Cayley trees, we find that ω_s decreases monotonically with RWC. However, as shown in Fig. 12, neither $P_{\max}$ nor $\langle P_s \rangle$ decrease with centrality. In fact there are noncentral vertices in $\mathrm{RHF}_{2,3}$ at which $P_{\max}$ and $\langle P_s \rangle$ attain a greater value than at the central vertex. This implies that $P_{\max}$ and $\langle P_s \rangle$ are not determined by the centrality of the vertex. It is remarkable to consider that the addition of these six vertices symmetrically about the central vertex can perturb the quantum walk dynamics to such an extent that the the relationship between centrality and $P_{\max}$ seen for Cayley trees is no longer maintained.

Figure 13 shows the results of the calculations for $n = 3$, $f = 3$ ($\mathrm{RHF}_{3,3}$; structure shown in Fig. 2). These results show that the overall trend is, again, decreasing ω_s with RWC but that the decrease is not monotonic. This implies that the search frequency on RHF is not determined solely by the centrality for some vertices. The vertices which break the trend have a particular structure; they are vertices which are connected by a single edge to a vertex which lies on a main path of the graph, so-called cul-de-sac vertices (highlighted in Fig. 2). The much smaller than expected values for ω_s at these cul-de-sac vertices is the first evidence that the local structure surrounding the marked vertex can greatly affect the frequency of the success probability. We now investigate this further.

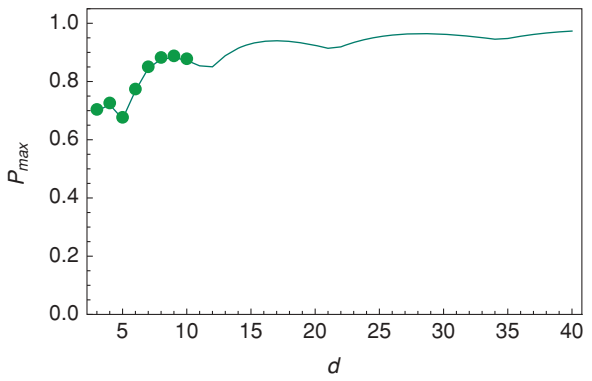

FIG. 9. (Color online) Analytical results for $P_{\max}$ on a second-generation Cayley tree with a central marked node as a function of branching rate d (solid line). Also plotted are numerical results (circles) obtained by direct simulation of quantum search for $3 \leqslant d \leqslant 10$.

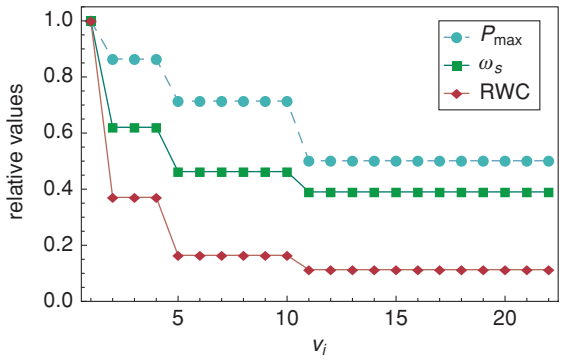

FIG. 10. (Color online) Numerical results for $P_{\max}$, ω_s, and RWC on the third-generation 3-Cayley tree (all data normalized for comparison). Data plotted as a function of vertex number v_i.

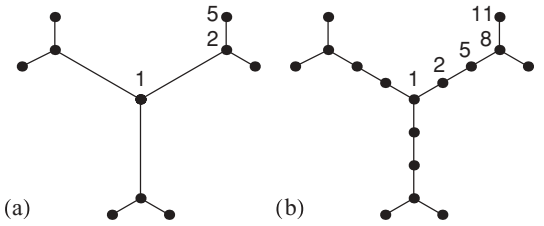

FIG. 11. A comparison of the structures of (a) the second-generation 3-Cayley tree and (b) $\mathrm{RHF}_{2,3}$. Vertices are ranked and labeled in order of decreasing random walk centrality.

We construct the graph $\mathrm{RHF}^{+}_{3,3}$ by adding a single extra vertex to $\mathrm{RHF}_{3,3}$ attached through a single edge to vertex 16, which is one of the cul-de-sac vertices in $\mathrm{RHF}_{3,3}$ (see Fig. 2). The calculated results for $P_{\max}$, ω_s, and RWC for $\mathrm{RHF}_{3,3}$ and $\mathrm{RHF}^{+}_{3,3}$ are listed in Table I. Note that in $\mathrm{RHF}_{3,3}$, vertices 14, 15, and 16 are structurally equivalent and have the same values for $P_{\max}$, ω_s, and RWC. The additional vertex attached to vertex 16 in $\mathrm{RHF}^{+}_{3,3}$ results in a decreasing RWC for that vertex. Given that the RWC is calculated using the relaxation time, this is expected. Since centrality is a relative measure among vertices, it is more informative to compare values within the same graph. We therefore compare values for vertex 16 with those for vertices 14 and 15, which are all equivalent in $\mathrm{RHF}_{3,3}$. For $\mathrm{RHF}^{+}_{3,3}$, we compute the ratios

$$\frac{P_{\max}^{(16)}}{P_{\max}^{(14,15)}} = 1.02,$$

$$\frac{\omega_s^{(16)}}{\omega_s^{(14,15)}} = 0.99,$$

$$\frac{\mathrm{RWC}^{(16)}}{\mathrm{RWC}^{(14,15)}} = 0.96,$$

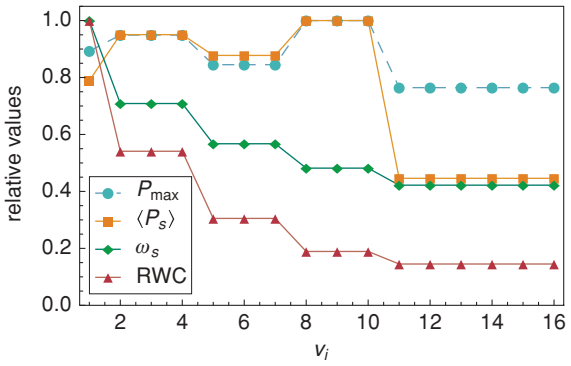

FIG. 12. (Color online) Numerical results for $P_{\max}$, ω_s, and $\langle P_s \rangle$ on $\mathrm{RHF}_{2,3}$. All data are normalized for comparison and vertices v_i are ordered with decreasing random walk centrality.

and we see that, in real terms, the effect of the node addition to vertex 16 is to decrease both ω_s and RWC. So we see, again, that ω_s appears to behave like RWC.

These data suggest that, for symmetric trees, ω_s is largely determined by RWC but the local structure surrounding the marked vertex *can* have a dramatic effect. It should be noted that all vertices in RHF which are observed to break the trend of decreasing ω_s with centrality have degree 1.

VII. QUANTUM SEARCH ON STRUCTURES WITH SIMPLE CYCLES

We now move away from trees to consider quantum-walk-based search on structures which contain simple cycles. In particular, we consider the Husimi cactus, the *joined* Cayley tree, and a Sierpiński gasket.

While a tree contains no simple cycles, a cactus is a graph in which any edge belongs to at most one simple cycle. In

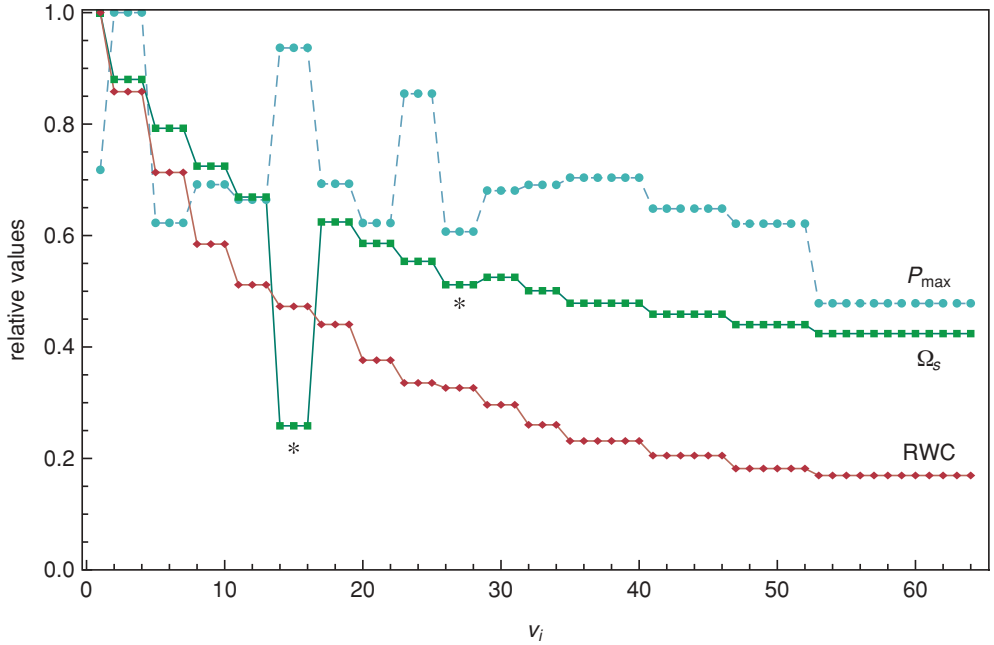

FIG. 13. (Color online) Numerical results for $P_{\max}$, ω_s, and RWC on $\mathrm{RHF}_{3,3}$. All data are normalized for comparison and vertices v_i are ordered with decreasing random walk centrality. The asterisk denotes sets of cul-de-sac vertices.

TABLE I. Changes in the values of P_{max}, ω_s, and RWC between $RHF_{3,3}$ and $RHF^{+}_{3,3}$, which has an extra vertex added to vertex 16 (see Fig. 2 for the structure of $RHF_{3,3}$).

	$RHF_{3,3}$	$RHF^{+}_{3,3}$	Change
$v_i = 14,15$			
P_{max}	2.065×10^{-1}	2.023×10^{-1}	-2.0%
ω_s	4.533×10^{-2}	4.574×10^{-2}	$+0.9\%$
RWC	1.166×10^{-3}	1.147×10^{-3}	-1.7%
$v_i = 16$			
P_{max}	2.065×10^{-1}	2.077×10^{-1}	$+0.6\%$
ω_s	4.533×10^{-2}	4.533×10^{-2}	0.0%
RWC	1.166×10^{-3}	1.106×10^{-3}	-5.4%

this sense, cacti are the most "treelike" graphs which contain simple cycles. In Husimi cacti derived from 3-Cayley trees, all simple cycles have length = 3. Studies of continuous-time quantum walks on these Husimi cacti have found that they display dynamics similar to that of Cayley trees [32]. Figure 14 shows ω_s, P_{max}, and RWC for the $N = 45$ Husimi cactus (structure shown in Fig. 4). As for the Cayley tree, it can be seen that the search frequency ω_s decreases with the centrality of the marked vertex. However, in contrast to the Cayley tree, P_{max} does not monotonically decrease with RWC. The results for the $N = 21$ Husimi cactus are analogous.

Figure 15 shows ω_s, P_{max}, and RWC for the joined Cayley tree of generation 3, with $d = 3$. We again see that ω_s and P_{max} generally decrease with centrality in a similar manner to the unjoined Cayley tree. In the joined graph (Fig. 3), vertices 11 and 12 are no longer structurally equivalent since vertex 11 lies in simple cycles of length = {3,7} and vertex 12 lies in simple cycles of length = {3,5}. It is shown in Fig. 15 that the search procedure for marked vertices 11 and 12 now produces different values for RWC, P_{max}, and ω_s. It should be noted that, for these vertices, P_{max} and RWC display the opposite trend to ω_s. This is different from the correlation observed on trees and Husimi cacti, where we saw that ω_s was usually highly correlated with RWC.

The results in Fig. 16 for the Sierpiński gasket show a relationship among P_{max}, ω_s, and centrality much more

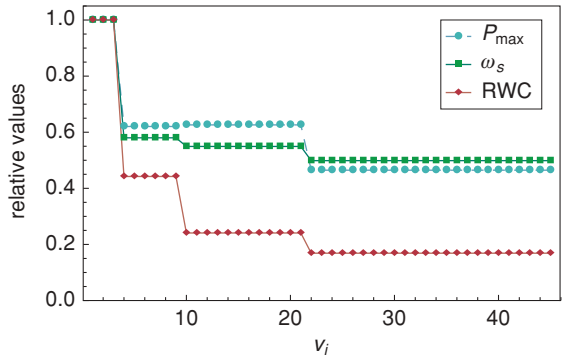

FIG. 14. (Color online) Numerical results for P_{max}, ω_s, and RWC on the Husimi cactus on $N = 45$ vertices. All data are normalized for comparison and vertices v_i are ordered according to decreasing RWC.

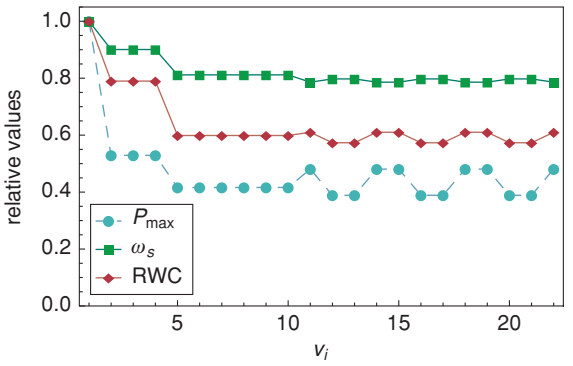

FIG. 15. (Color online) Numerical results for P_{max}, ω_s, and RWC on the third-generation joined 3-Cayley tree (all data normalized for comparison). Data plotted as a function of vertex number v_i, which is derived from the numbering of the unjoined Cayley tree. Note that vertices 11 and 12 are no longer equivalent in the joined Cayley tree.

complex than that seen for the other structures studied. We expect that the presence of simple cycles of various lengths in the structure results in interesting interference effects in quantum walks on these graphs. This interference produces much more complex behavior of $P_s(t)$, which makes any relationship between $P_s(t)$ and the centrality of the marked vertex harder to observe. As shown in in Fig. 16 that the peripheral (least central) vertices do not produce the smallest values of P_{max} or ω_s in this case.

VIII. DISCUSSION AND CONCLUSIONS

We have demonstrated that the quantum search procedure for a marked vertex in a Cayley tree results in a time-dependent success probability $P_s(t)$ that attains a greater maximum value and has a higher minimum frequency for marked vertices which are more central. Our study was extended to RHFs, where it was found that the maximum value of $P_s(t)$ does not necessarily decrease with centrality. We also found that the minimum frequency of the search probability ω_s on RHFs

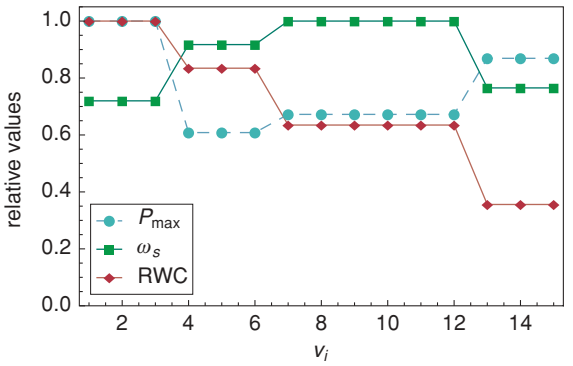

FIG. 16. (Color online) Numerical results for P_{max}, ω_s, and RWC on the second-generation Sierpiński gasket. All data are normalized for comparison and vertices v_i are ordered according to decreasing RWC.

is strongly related to centrality and that exceptions to this trend are caused by the *local* structure surrounding the marked vertex. We therefore conclude that the success probability $P_s(t)$ for a marked vertex in a highly symmetric tree contains information about the global structure of the tree and the overall position of the marked vertex within the tree. It also contains information regarding the local structure surrounding the marked vertex.

We say that two vertices are *structurally equivalent* if they have the same structural relationship to all of the other vertices of the graph (e.g., in a Cayley tree, all vertices which are a given distance from the center are equivalent). We then note that all equivalent vertices in the graphs studied in this work have the same values of $P_{\max}$ and ω_s and all inequivalent vertices have different values, suggesting that $P_{\max}$ and ω_s could be used to partition the vertex set into structural equivalence classes. It should be noted, however, that this partitioning would not be possible for all graphs, since strongly regular graphs contain inequivalent vertices that produce identical success probabilities. These graphs therefore give identical values for ω_s and $P_{\max}$ for inequivalent vertices. We find that for all vertices of degree >1 in the trees and cacti studied here, ω_s can be used to order the vertices with decreasing centrality, as measured by the RWC.

The RWC considered in this paper is an example of a *closeness* centrality measure; that is, it measures the closeness of a vertex to the center of the graph. There are, however, other classes of centrality measures [22]. One of these is *betweenness* centrality, which represents the capacity of a vertex in a network to withhold information if it were removed from the network [22]. While betweenness and closeness are equivalent for Cayley trees, this is not true for RHFs. As seen in the studies on RHFs, the values of ω_s obtained for the cul-de-sac vertices were unusually low compared with the corresponding values of the RWC. This could be related to the low betweenness centrality of these vertices. It would be an interesting subject for further study to investigate the relationship between characteristics of $P_s(t)$ and other measures of centrality.

It is also worth noting that $P_s(t)$ can be classically computed with time complexity $O(tN^2 \log N)$, where t is the simulation time and N is the number of vertices. Therefore, ω_s can be classically computed with time complexity $O(t^2 \log(tN^2) \log N)$. Numerically, we find that for a 1% error in ω_s for typical values of ω_s on a 3-Cayley tree, $t \approx O(N^{0.7})$ and thus the time complexity becomes $O(N^{3.4}(\log N)^2)$. This is comparable with the complexity of the equivalent RWC calculation, which scales as $O(tN^2) \approx O(N^{3.1})$.

It is evident that a tremendous amount of information about the structure of the graph and the overall position of the marked vertex is present in $P_s(t)$, and we suggest that the "lowest frequency" considered here is perhaps the simplest example of extracting this information. We propose that it would be extremely interesting to consider more detailed Fourier analysis of $P_s(t)$ to uncover the origin of the other frequencies present and hence determine what other information is obtainable. It would also be interesting to determine if the centrality information, which was easy to obtain via ω_s in the case of simple symmetric trees, can be extracted for more complex cases.

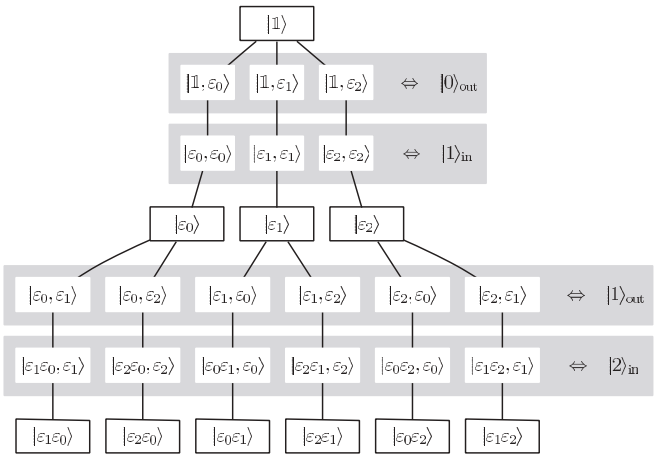

FIG. 17. Second-generation 3-Cayley tree, shown with the vertex states $|g\rangle \in \mathcal{H}_{\mathcal{P}}$ and the subnode states $|g,\varepsilon\rangle \in \mathcal{H}_{\mathcal{P}} \otimes \mathcal{H}_{\mathcal{C}}$. Shaded regions enclose groups of subnode states that make up $\{|x\rangle_{\text{out}}, |x\rangle_{\text{in}}\}$, shown on the right.

ACKNOWLEDGMENTS

The authors would like to thank Brendan Douglas for helpful discussions as well as the referee for constructive comments, in particular, the suggestion to study the Husimi cactus.

APPENDIX: ANALYTICAL RESULTS FOR ω_s ON CAYLEY TREES

We map the quantum walk on a Cayley tree to a finite one-dimensional quantum walk and derive an expression for ω_s when the central vertex is marked for $n = 2,3$. The first part of the analysis follows the method of Chisaki *et al.* [27], however, the time-evolution operator used here is modified to incorporate the marking operator and reflection at the surface vertices (Chisaki *et al.* consider an infinite tree). The initial state is also different, therefore the complete derivation is presented.

1. Defining the discrete-time quantum walk on a Cayley tree

An nth-generation Cayley tree of order d is an undirected graph in which every vertex is connected to d others except for vertices at a distance n from the center. The vertex set V is defined as the group of elements generated by the set $\Sigma = \{\varepsilon_0, \ldots, \varepsilon_{d-1}\}$ with the constraint ${\varepsilon_i}^2 = \mathbb{1}, i = 0, \ldots, d-1$,

$$V = \{\varepsilon_{i_k}\varepsilon_{i_{k-1}}\ldots\varepsilon_{i_2}\varepsilon_{i_1} \;:\; 0 \leqslant k \leqslant n, \quad \varepsilon_{i_j} \in \Sigma, \quad \text{and} \quad i_{j+1} \neq i_j \quad \text{for} \quad j = 1,2,\ldots,k-1\}.$$

The *reduced word length* $|g|$ of a vertex g is the number of elements used when g is written as a reduced product of $\varepsilon_i \in \Sigma$ (e.g., $|\varepsilon_2\varepsilon_2\varepsilon_1\varepsilon_0\varepsilon_2| = |\mathbb{1}\varepsilon_1\varepsilon_0\varepsilon_2| = |\varepsilon_1\varepsilon_0\varepsilon_2| = 3$). Using this construction, the vertices at level k in the tree have $|g| = k$. Vertices g and h are connected if and only if $gh^{-1} \in \Sigma$. This is illustrated in Fig. 17.

The quantum walk takes place on the subnodes of the graph which belong to the Hilbert space $\mathcal{H}_{\mathcal{P}} \otimes \mathcal{H}_{\mathcal{C}}$. We write these states $\{|g,\varepsilon_j\rangle : g \in V, \varepsilon_j \in \Sigma\}$. In this basis the action

of the unitary Grover coin and shift operators which drive the quantum walk can be written as

$$(\mathbb{1}\otimes C)|g,\varepsilon\rangle = \begin{cases} \sum_{\tau\in\Sigma}(-\delta_{\varepsilon\tau}+2/d)|g,\tau\rangle, & |g|<n, \\ |g,\varepsilon\rangle, & |g|=n, \end{cases} \tag{A1}$$

$$S|g,\varepsilon\rangle = |\varepsilon g,\varepsilon\rangle. \tag{A2}$$

The coin operator [Eq. (A1)] applies a Grover coin to all vertices except those at the surface, which are left unchanged, while the shift operator [Eq. (A2)] swaps the probability amplitudes between connected subnodes. With the perturbed time evolution operator $U' := S(\mathbb{1}\otimes C')$, one step of the discrete-time quantum walk on the Cayley tree becomes

$$U'|g,\varepsilon\rangle = \begin{cases} \sum_{\tau\in\Sigma}(-\delta_{\varepsilon\tau}+2/d)|\tau g,\tau\rangle, & |g|<n, \quad g\notin M, \\ |\varepsilon g,\varepsilon\rangle, & |g|=n, \quad g\notin M, \\ -|\varepsilon g,\varepsilon\rangle, & g\in M. \end{cases} \tag{A3}$$

2. Mapping the quantum walk on a Cayley tree to a quantum walk on a finite line

As described in [23], [24], [27], and [29], in certain cases, the symmetry of the initial state allows us to map the quantum walk on a Cayley tree to a walk on a line. Define the sets

$$E^+(x) = \{(g,\varepsilon)\in V\times\Sigma : |g|=x, |\varepsilon g|=x+1\},$$
$$E^-(x) = \{(g,\varepsilon)\in V\times\Sigma : |g|=x, |\varepsilon g|=x-1\},$$

and consider the subspace $\mathcal{H}'\subset\mathcal{H}$ spanned by the states

$$|x\rangle_{\text{out}} = \frac{1}{\sqrt{d(d-1)^x}}\sum_{(g,\varepsilon)\in E^+(x)}|g,\varepsilon\rangle, \quad 0\leqslant x\leqslant n-1,$$

$$|x\rangle_{\text{in}} = \frac{1}{\sqrt{d(d-1)^{x-1}}}\sum_{(g,\varepsilon)\in E^-(x)}|g,\varepsilon\rangle, \quad 1\leqslant x\leqslant n,$$

as shown in Fig. 17. If the initial state $|\Psi_0\rangle$ of the quantum walk on a Cayley tree is an equal superposition of all vertex states, equally divided among the subnodes of each vertex,

$$|\Psi_0\rangle = \sqrt{\frac{d-2}{(d\times(d-1)^n-2)}}\sum_{g\in V}\sum_{\varepsilon:|\varepsilon g|<n}\frac{1}{\sqrt{d(g)}}|g,\varepsilon\rangle, \tag{A4}$$

where $d(g)$ is the degree of the vertex, then $|\Psi_0\rangle$ can be written as a superposition of $\{|x\rangle_{\text{out}},|x\rangle_{\text{in}}\}$:

$$|\Psi_0\rangle = \sqrt{\frac{d-2}{d\times(d-1)^n-2}}\left(\sum_{x=0}^{n-1}\sqrt{(d-1)^x}|x\rangle_{\text{out}} + \sum_{x=1}^{n-1}\sqrt{(d-1)^{x-1}}|x\rangle_{\text{in}} + \sqrt{d(d-1)^{n-1}}|n\rangle_{\text{in}}\right). \tag{A5}$$

We now specialize to the case where there is a single marked vertex at the center of the tree ($M=\{\mathbb{1}\}$) and consider the action of U' on the subspace $\mathcal{H}'\subset\mathcal{H}_{\mathcal{P}}\otimes\mathcal{H}_{\mathcal{C}}$.

For $1\leqslant x\leqslant n$,

$$U'|x\rangle_{\text{in}} = \left(\frac{2}{d}-1\right)|x-1\rangle_{\text{out}} + \frac{2\sqrt{d-1}}{d}|x+1\rangle_{\text{in}}, \tag{A6}$$

$$U'|x\rangle_{\text{out}} = -\left(\frac{2}{d}-1\right)|x+1\rangle_{\text{in}} + \frac{2\sqrt{d-1}}{d}|x-1\rangle_{\text{out}}, \tag{A7}$$

and on the boundaries,

$$U'|0\rangle_{\text{out}} = -|1\rangle_{\text{in}}, \tag{A8}$$

$$U'|n\rangle_{\text{in}} = |n-1\rangle_{\text{out}}. \tag{A9}$$

Note that $|\Psi_0\rangle\in\mathcal{H}'\Rightarrow|\Psi(t)\rangle=(U')^t|\Psi_0\rangle\in\mathcal{H}', \forall\, t\in\mathbb{Z}^+$.

From this subspace the quantum walk on the tree can be mapped to a quantum walk on a finite line with reflecting boundaries. Define the Hilbert space $\widetilde{\mathcal{H}}=\{|x,A\rangle : x\in\mathbb{Z}^+, A\in\{L,R\}\}$ and the subspace $\widetilde{\mathcal{H}}'\subset\widetilde{\mathcal{H}}$ spanned by $\{|0,L\rangle,|1,R\rangle,|1,L\rangle,\ldots,|n-1,R\rangle,|n-1,L\rangle,|n,R\rangle\}$. Now consider the 1-1 association $\mathcal{H}'\leftrightarrow\widetilde{\mathcal{H}}'$ defined by

$$|x\rangle_{\text{out}}\leftrightarrow|x,L\rangle, \qquad |x\rangle_{\text{in}}\leftrightarrow|x,R\rangle. \tag{A10}$$

We also map the operator $U'\leftrightarrow\widetilde{U}'$ so that the action of U' on the states $\{|x\rangle_{\text{in}},|x\rangle_{\text{out}}\}$ is equivalent to the action of $\widetilde{U}'$ on the states $\{|x,R\rangle,|x,L\rangle\}$. The quantum walk on a Cayley tree subject to the foregoing conditions is then seen to be equivalent to a finite one-dimensional quantum walk with a biased coin and asymmetric initial distribution.

Using the mapping (A10), we can express (A6)–(A9) in the new basis by defining $\widetilde{U}' := \widetilde{S}(\mathbb{1}\otimes\widetilde{C})$, where $\widetilde{C}=\widetilde{C}(x)$ is defined by

$$(\mathbb{1}\otimes\widetilde{C})|x,A\rangle = |x\rangle\otimes H(x)|A\rangle, \tag{A11}$$

where

$$H(x) = \begin{cases} -\sigma_1, & x=0, \\ h, & 0<x<n, \\ \sigma_1, & x=n, \end{cases}$$

$$h = \begin{pmatrix} \frac{2\sqrt{d-1}}{d} & \frac{2}{d}-1 \\ -\left(\frac{2}{d}-1\right) & \frac{2\sqrt{d-1}}{d} \end{pmatrix}, \quad \sigma_1 = \begin{pmatrix} 0 & 1 \\ 1 & 0 \end{pmatrix}.$$

$\widetilde{S}$ acts on $\widetilde{\mathcal{H}}'$ as follows:

$$\widetilde{S}|x,A\rangle = \begin{cases} |x+1,R\rangle, & A=R, \\ |x-1,L\rangle, & A=L. \end{cases} \tag{A12}$$

It can thus be seen that the quantum walk on the Cayley tree with a central marked vertex starting with equal probability at all vertices is equivalent to a quantum walk on a finite line with a perfectly reflecting boundary at $x=n$ and a π phase shift upon reflection at $x=0$. The reflections are achieved by careful choice of the coin operator.

3. Analytical results for $P_s(t)$ and ω_s for the second-generation Cayley tree

Consider the second-generation d-Cayley tree with a central marked vertex. Let B be a matrix representation of $\widetilde{U}'$ on the

complete, orthonormal basis $\{|0,L\rangle,|1,R\rangle,|1,L\rangle,|2,R\rangle\}$ of $\widetilde{\mathcal{H}}'$. Let $|\phi_i\rangle \in \{|0,L\rangle,|1,R\rangle,|1,L\rangle,|2,R\rangle\}$; then

$$(B_{ij}) = (\langle\phi_i|\widetilde{U}'|\phi_j\rangle) = \begin{pmatrix} 0 & \frac{2}{d}-1 & \frac{2\sqrt{d-1}}{d} & 0 \\ -1 & 0 & 0 & 0 \\ 0 & 0 & 0 & 1 \\ 0 & \frac{2\sqrt{d-1}}{d} & 1-\frac{2}{d} & 0 \end{pmatrix},$$

where the states are ordered as above.

We would like to find a closed-form expression for $|\Psi(t)\rangle = (\widetilde{U}')^t|\Psi_0\rangle$. In particular, we are interested in the probability of finding the walker at the central marked vertex as a function of time,

$$|\Psi(t)\rangle = (\widetilde{U}')^t|\Psi_0\rangle,$$
$$\langle\phi_i|\Psi(t)\rangle = \sum_j \langle\phi_i|(\widetilde{U}')^t|\phi_j\rangle\langle\phi_j|\Psi_0\rangle,$$

which can be written in matrix form as

$$c_i(t) = (B_{ij})^t c_j(0), \tag{A13}$$

where $c_i(t) := \langle\phi_i|\Psi(t)\rangle$ are column vectors. Since $\widetilde{U}'$ is a unitary operator and the basis $|\phi_i\rangle$ is orthonormal, it follows that B is a 4×4 unitary matrix and therefore has four distinct eigenvalues of unit norm corresponding to four orthonormal eigenvectors [34]. Furthermore, B is unitary similar to the diagonal matrix D, which contains the eigenvalues of B as its diagonal elements. Let P be the unitary matrix containing the eigenvectors of B as its columns. From Eq. (A13) and the unitarity of P,

$$P^{\dagger}{}_{ki}c_i(t) = P^{\dagger}{}_{ki}(B_{ij})^t P_{jl}P^{\dagger}{}_{lj}c_j(0),$$
$$P^{\dagger}{}_{ki}c_i(t) = (P^{\dagger}{}_{ki}B_{ij}P_{jl})^t P^{\dagger}{}_{lj}c_j(0),$$
$$P^{\dagger}{}_{ki}c_i(t) = (D_{kl})^t P^{\dagger}{}_{lj}c_j(0).$$

Now, writing $P^{\dagger}{}_{ki}c_i(t) =: v_k(t)$, we have

$$v_k(t) = (D_{kl})^t v_l(0). \tag{A14}$$

But $D = \mathrm{diag}(\lambda_k)$, where λ_k are the eigenvalues of B. So $D_{kl} = 0$ for $k \neq l \Rightarrow v_k(t) = (D_{kk})^t v_k(0)$ or, equivalently,

$$v_k(t) = {\lambda_k}^t v_k(0). \tag{A15}$$

The eigenvalues of B are

$$\lambda_k = \pm e^{\pm\Omega/2}, \quad \text{where} \quad \Omega = \arctan\left(\frac{2\sqrt{d-1}}{d-2}\right). \tag{A16}$$

We can now solve for the time evolution of $v_k(t)$ for $k = 1,\ldots,4$ and use P to find $c_k(t) := \langle\phi_k|\Psi(t)\rangle$, from which we obtain $\langle\mathbb{1}|\Psi(t)\rangle$. The eigenvalues are found by diagonalizing B; that is,

$$D = P^{\dagger}BP = \mathrm{diag}(-e^{-i\Omega/2},-e^{i\Omega/2},e^{i\Omega/2},e^{-i\Omega/2}), \tag{A17}$$

where the unitary change of basis matrix P contains the orthonormal eigenvectors of B as its columns:

$$P = \frac{1}{2}\begin{pmatrix} i & -i & -i & i \\ ie^{i\Omega/2} & -ie^{-i\Omega/2} & ie^{-i\Omega/2} & -ie^{i\Omega/2} \\ -e^{i\Omega/2} & -e^{-i\Omega/2} & e^{-i\Omega/2} & e^{i\Omega/2} \\ 1 & 1 & 1 & 1 \end{pmatrix}. \tag{A18}$$

The probability amplitude at the central (marked) vertex is thus

$$\begin{aligned}\langle\mathbb{1}|\Psi(t)\rangle \equiv \langle 0,L|\Psi(t)\rangle = c_1(t) &= \sum_i P_{1i}v_i(t) \\ &= \frac{1}{2}[i(-e^{-i\Omega/2})^t v_1(0) - i(-e^{i\Omega/2})^t v_2(0) \\ &\quad - ie^{i\Omega t/2}v_3(0) + ie^{-i\Omega t/2}v_4(0)],\end{aligned}$$

where $v_i(0)$ represent the initial state in the eigenvector basis and are found using Eq. (A5) and the unitary transformation $P^{\dagger}$. Taking the absolute value squared,

$$\begin{aligned}|\langle\mathbb{1}|\Psi(t)\rangle|^2 = \tfrac{1}{4}\{|\mathbf{v}|^2 &+ 2\mathrm{Re}(v_1\bar{v}_4 + v_2\bar{v}_3)\cos(\pi t) \\ &- 2\mathrm{Re}(v_1\bar{v}_2 + \bar{v}_3v_4)\cos(\Omega t) \\ &- 2\mathrm{Im}(v_1\bar{v}_2 + \bar{v}_3v_4)\sin(\Omega t) \\ &- 2\mathrm{Re}(v_1\bar{v}_3 + \bar{v}_2v_4)\cos[(\pi-\Omega)t] \\ &+ 2\mathrm{Im}(v_1\bar{v}_3 + \bar{v}_2v_4)\sin[(\pi-\Omega)t]\}.\end{aligned}$$

We now see that the lowest frequency in the success probability $\omega_s = \Omega$. The initial condition [Eq. (A5)] can be converted to the eigenvector basis and the expression [Eq. (A16)] for $\Omega(d)$ can then be used to solve for v_i. Upon simplification, we obtain Eq. (9) (Sec. V B), valid for $3 \leqslant d < \infty$.

4. Analytical results for $P_s(t)$ and ω_s for the third-generation Cayley tree

We perform the same analysis for the case $n = 3$, where this time $\widetilde{U}'$ induces a 6×6 matrix B. We find that the eigenvalues of B are

$$\lambda_k = \pm i, \pm e^{\pm\Omega/2}, \quad \text{where} \quad \Omega = \arctan\left(\frac{2\sqrt{d^2-1}}{d^2-2}\right). \tag{A19}$$

As in the previous case, the eigenvalues of B uniquely determine the frequencies present in $P_s(t)$. Since $i = e^{i\pi/2}$ and $\Omega < \pi/2$ for $3 \leqslant d < \infty$, it follows that $\omega_s = \Omega$.

[1] J. Kempe, Contemp. Phys. **44**, 307 (2003).
[2] V. Kendon, Math. Struct. Comp. Sci. **17**, 1169 (2007).
[3] M. Santha, Lect. Notes Comput. Sci. **4978**, 31 (2008).
[4] J. Smith and M. Mosca, e-print arXiv:1001.0767v2 [quant-ph].
[5] M. Katori, S. Fujino, and N. Konno, Phys. Rev. A **72**, 012316 (2005).
[6] T. Oka, N. Konno, R. Arita, and H. Aoki, Phys. Rev. Lett. **94**, 100602 (2005).
[7] P. Kurzynski, Phys. Lett. A **372**, 6125 (2008).
[8] Q.-K. Meng and J.-Y. Zhu, Chinese Phys. B **18**, 3632 (2009).
[9] M. A. Broome, A. Fedrizzi, B. P. Lanyon, I. Kassal, A. Aspuru-Guzik, and A. G. White, Phys. Rev. Lett. **104**, 153602 (2010).

[10] L. K. Grover, Phys. Rev. Lett. **79**, 325 (1997).
[11] L. K. Grover, Phys. Rev. Lett. **79**, 4709 (1997).
[12] N. Shenvi, J. Kempe, and K. B. Whaley, Phys. Rev. A **67**, 052307 (2003).
[13] A. Ambainis, J. Kempe, and A. Rivosh, in *SODA '05: Proceedings of the Sixteenth Annual ACM-SIAM Symposium on Discrete Algorithms* (Society for Industrial and Applied Mathematics, Philadelphia, PA, 2005), pp. 1099–1108.
[14] D. Reitzner, M. Hillery, E. Feldman, and V. Bužek, Phys. Rev. A **79**, 012323 (2009).
[15] A. M. Childs and J. Goldstone, Phys. Rev. A **70**, 022314 (2004).
[16] E. Agliari, A. Blumen, and O. Mülken, Phys. Rev. A **82**, 012305 (2010).
[17] D. Aharonov, A. Ambainis, J. Kempe, and U. Vazirani, in *STOC '01: Proceedings of the Thirty-third Annual ACM Symposium on Theory of Computing* (ACM, New York, 2001), pp. 50–59.
[18] V. Kendon and B. C. Sanders, Phys. Rev. A **71**, 022307 (2005).
[19] B. L. Douglas and J. B. Wang, J. Phys. A **41**, 075303 (2008).
[20] J. D. Noh and H. Rieger, Phys. Rev. Lett. **92**, 118701 (2004).
[21] D. A. Levin, Y. Peres, and E. L. Wilmer, *Markov Chains and Mixing Times*, 1st ed. (American Mathematical Society, Providence, RI, 2008).
[22] S. P. Borgatti and M. G. Everett, Social Networks **28**, 466 (2006).
[23] A. M. Childs, R. Cleve, E. Deotto, E. Farhi, S. Gutmann, and D. A. Spielman, in *STOC '03: Proceedings of the Thirty-fifth Annual ACM Symposium on Theory of Computing* (ACM, New York, 2003), pp. 59–68.
[24] O. Mülken, V. Bierbaum, and A. Blumen, J. Chem. Phys. **124**, 124905 (2006).
[25] E. Agliari, A. Blumen, and O. Mülken, J. Phys. A **41**, 445301 (2008).
[26] E. Farhi and S. Gutmann, Phys. Rev. A **58**, 915 (1998).
[27] K. Chisaki, M. Hamada, N. Konno, and E. Segawa, Interdis. Inform. Sci. **15**, 423 (2009).
[28] B. Tregenna, W. Flanagan, R. Maile, and V. Kendon, New J. Phys. **5**, 83 (2003).
[29] I. Carneiro, M. Loo, X. Xu, M. Girerd, V. Kendon, and P. L. Knight, New J. Phys. **7**, 156 (2005).
[30] X.-P. Xu, J. Phys. A **42**, 115205 (2009).
[31] A. Volta, J. Phys. A **42**, 225003 (2009).
[32] A. Blumen, V. Bierbaum, and O. Mülken, Physica A **371**, 10 (2006).
[33] M. Barlow and E. Perkins, Prob. Theory Relat. Fields **79**, 543 (1988).
[34] S. Hassani, *Mathematical Physics: A Modern Introduction to Its Foundations* (Springer, New York, 1998).